



HAL
open science

Ultrasonic monitoring of stress and cracks of the 1/3 scale mock-up of nuclear reactor concrete containment structure

Qi Xue, Éric Larose, Ludovic Moreau, Romain Theyry, Odile Abraham,
Jean-Marie Henault

► **To cite this version:**

Qi Xue, Éric Larose, Ludovic Moreau, Romain Theyry, Odile Abraham, et al.. Ultrasonic monitoring of stress and cracks of the 1/3 scale mock-up of nuclear reactor concrete containment structure. Structural Health Monitoring, 2021, 10.1177/14759217211034729 . hal-03313112

HAL Id: hal-03313112

<https://hal.science/hal-03313112>

Submitted on 3 Aug 2021

HAL is a multi-disciplinary open access archive for the deposit and dissemination of scientific research documents, whether they are published or not. The documents may come from teaching and research institutions in France or abroad, or from public or private research centers.

L'archive ouverte pluridisciplinaire **HAL**, est destinée au dépôt et à la diffusion de documents scientifiques de niveau recherche, publiés ou non, émanant des établissements d'enseignement et de recherche français ou étrangers, des laboratoires publics ou privés.

Ultrasonic monitoring of stress and cracks of the 1/3 scale mock-up of nuclear reactor concrete containment structure

Journal Title
XX(X):1-8
©The Author(s) 2016
Reprints and permission:
sagepub.co.uk/journalsPermissions.nav
DOI: 10.1177/ToBeAssigned
www.sagepub.com/

SAGE

Qi Xue¹, Eric Larose¹, Ludovic Moreau¹, Romain Thery^{1,2}, Odile Abraham², Jean-Marie Henault³

Abstract

To evaluate the stress level and damage of a reinforced concrete containment wall (similar to those used in nuclear power plants) and its reaction to pressure variations, we implemented successive ultrasonic experiments on the exterior surface of the containment wall in the gusset area for three consecutive years (2017, 2018 and 2019). During each experiment, the pressure inside the containment wall increased gradually from 0 MPa to 0.43 MPa and then decreased back to 0 MPa. From the analysis of the ultrasonic coda waves obtained in the multiple scattering regime (80-220 kHz), we performed Coda Wave Interferometry to calculate the apparent velocity changes in the structure (denoted by dV/V_a) and Coda Wave Decorrelation (DC) measurements to produce 3D cartographies of stress and crack distribution. From three source-receiver pairs, located at the top, middle and bottom of the experimental region, we observe that coda waves dilate, shrink and remain almost unchanged, respectively. This corresponds to the decreasing, increasing and invariant pressure inside the concrete. The comparison of three years' results demonstrates that the variation of dV/V_a and DC under the same pressure test increases through the years, which indicates the progressive deterioration and aging of the concrete. From a large collection of source-receiver pairs at different times, the spatial-temporal variations of dV/V_a and DC are then used to produce a map of the structural velocity and scattering changes, respectively. We observe a decreasing velocity on the top part and an increasing in the middle one, which is in line with the dV/V_a analysis. The reconstructed scattering changes (or structural changes) highlight the active region during the inflation-deflation procedure, corresponding to the opening and closing (and sometimes the development) of cracks. The larger magnitude in 2019 than in 2017 indicates the increasing damage in the concrete.

Keywords

Coda wave interferometry, diffuse ultrasound, cracks in concrete, velocity change, stretching and correlation

Introduction

Concrete containments are generally used to protect the nuclear reactor of a nuclear power plant in case of any leakage of the nuclear fuel or waste, or from possible external aggression. The humidity, temperature and/or pressure changes induce the deformation of the concrete shell and, together with additional chemical processes, progressively alter the mechanical integrity of the structure. Small cracks (millimeter scale) are generated and progressively develop during the lifetime of the structure. The assessment of the state of damage and the characterization of cracks are vital issues for the security of the nuclear power plant in case of emergency, and for the estimation of the residual life time. In France, a leak test of each concrete containment is enforced by the law every ten years¹, during which the pressure inside the containment is increased from 0 MPa to about 0.43 MPa and then decreased back to 0 MPa.

In order to study the aging of the concrete wall and follow the evolution of the leak rate owing to drying creep and loss of pre-stress in a realistic environment, Électricité de France (EDF) launched a research program

on a 1/3 scale mock-up, called VeRCoRs²⁻⁴. This mock-up is a double walled concrete containment building, as a 1/3 scale specimen representative for 24 (about 40%) of the French reactors. The present work explores the applicability and performance of a method based on diffuse ultrasound analysis to image and quantify stress changes and cracks within the structure at VeRCoRs during a standard internal pressure test.

To this end, we take advantage of the high sensitivity of multiply scattered waves at the ultrasonic scale, for frequencies of few hundreds of kHz. The high heterogeneity of the concrete results in the loss of ballistic and coherent properties of the waveforms after a propagation over a few wavelengths. The waveforms of the late-arriving ultrasonic signals, also known as coda waves,

¹Univ. Grenoble Alpes, CNRS, ISTERRE, CS 40700, 38058 Grenoble, France

²Uni. Eiffel, GERS-GeoEND, allée des ponts et chaussées - CS5004, 44344 Bouguenais Cedex, FRANCE

³ EDF R&D, Chatou, France

Corresponding author:

Éric Larose, ISTERRE, Grenoble, France.

Email: eric.larose@univ-grenoble-alpes.fr

are known to be highly reproducible for a fixed source and receiver, while being very sensitive to small perturbation of the medium. At the seismic scale, the sensitivity of the coda wave has been extensively exploited to detect small changes in the Earth's crust, e.g., fault zones^{5,6} or volcanic areas⁷⁻⁹.

Coda wave interferometry (CWI), as introduced in¹⁰ and further developed in^{11,12}, is a technique to detect slight velocity perturbations in a highly heterogeneous medium, by comparing coda waves recorded before and after a perturbation. A quantitative way to compare two waveforms is to compute their correlation coefficient (CC). One way of applying CWI consists in stretching or shrinking the waveform to match two coda signals, i.e., to maximize the CC in a given time window, with a dilation coefficient. This coefficient, associated to the local velocity change¹³, is generally referred to as the apparent relative velocity change dV/V_a . Alternatively, it can be useful to calculate the DC instead of the CC, because the DC can be linked to small structural changes¹⁴. The dV/V_a and DC variables are now widely used to detect ultrasonic velocity changes in a concrete structure induced by thermal or stress variations¹⁵⁻¹⁷, and/or to detect micrometer scale cracks¹⁸. The reader can refer to¹⁹ for a review.

The relation between the dV/V_a and the local velocity change is proposed in²⁰ by comparing wave propagation with random walk. The relation between DC and the local scattering change (for example, induced by cracks) follows a similar formula proposed later²¹. The reader may refer to²² for a detailed explanation and proof. These two formulas have the same form: an integral equation with the same sensitivity kernel. The sensitivity kernel is a function of the source, receiver, space and time, that statistically estimates the density of time spent by the diffuse wave at a given region of the medium. It can be estimated either from i) the explicit solution of diffusive or radiative-transfer approximation of ultrasonic waves for simple geometries (e.g., infinite plate or cuboid)²², ii) numerical methods (e.g., finite difference or finite element) for any shape²³ or iii) directly solving the wave equation²⁴. By combining information from several sources and receivers, we are able to obtain thousands of dV/V_a and DC values between different source-receiver pairs in different times, which can be used to image the velocity and scattering changes through solving the integral equation. Please refer to¹⁴ for a numerical simulation,²⁵ and²⁶ for laboratory experiments and²⁷ for a field experiment.

We implemented similar diffuse ultrasonic experiments on the outer surface of the gusset area of VeRCoRs (see Fig. 1(a)) during the internal pressure test over three consecutive years, in order to detect cracks and the effect of damage on stress changes during each test. From the analysis of the dV/V_a and DC for three different source-receiver pairs between the initial state and other states during the pressure test, we aim at observing that different parts of the wall are expected to have different responses to the same inflation-deflation procedure. We also aim at quantifying the evolution of dV/V_a and DC versus aging and damage over the years. An imaging inversion procedure is then applied to obtain 3D cartographies of

relative velocity changes and density of probability of cracks.

The comparison of different years' results may quantify the deterioration of the concrete: the sensitivity of dV/V_a to internal stress is expected to increase with time (thus with damage) as observed elsewhere¹⁹ and the decorrelation is expected to show some non-reversible (thus cumulative) behavior.

Experimental setup

VeRCoRs is a 1/3 scale experimental mock-up of a nuclear reactor containment (see Fig. 1(a)) built by EDF near Paris. Construction of the mock-up began in 2013 and was completed in March 2016. The construction procedure is layer by layer. The horizontal dashed lines in Fig. 1(b) and (c) indicate positions of the joint in our experimental region. After the construction, two auxiliary air-conditioning units started to impose relative realistic humidity and temperature inside and outside the containment to simulate regular operations of a nuclear reactor. The 1/3 scale was chosen to accelerate aging, ten times faster than in a realistic environment hopefully²⁸.

To monitor the properties of the concrete, the pressure inside the structure increases gradually from 0 MPa to 0.43 MPa, which is followed by a static period, during which the pressure decreases a little bit due to small leakage from cracks, and then the whole structure is deflated to its initial state (see Fig. 2(a)). This test was repeated several times, twice in 2017, and once in 2018 and 2019, which corresponds to the standard leak test for real nuclear power plant containment every ten years. We foresee a large change of the concrete in the first test in 2017, because it was the first pressure test and a lot of micro and macro-cracks were created. Therefore, in this paper we only present the second test in 2017, to take into account the so-called Kaiser effect that has been observed and commented previously in concrete²⁹. Modifications observed in the following are thus not related to the fact that the pressure level exceeds the first one. Our experiment was implemented on the outer surface of the gusset region (a surface of about 2m×2m). Fig. 1(a) provides a sketch of the structure and the experimental region.

Several transducers are glued directly to the concrete to generate and receive ultrasonic signals. Fig. 1(b) shows the positions of sources and receivers in 2017 and 2018, and Fig. 1(c) shows positions in 2019. Since the base of the concrete structure (base slab) is extremely thick, the signals recorded by the bottom source-receiver pair (S12-R12) remain almost unchanged during the experiment in 2017 and 2018. We decided to remove them and to add several new transducers to improve the resolution of the upper part in 2019. In addition, we did not receive reasonable signals from R1 in 2018 which may be caused by the failure or detachment of the transducer.

During the experiment, a chirp signal with frequency ranging from 80 to 220 kHz is generated, amplified and sent into the concrete from each source one after another, and then recorded by all the receivers in order

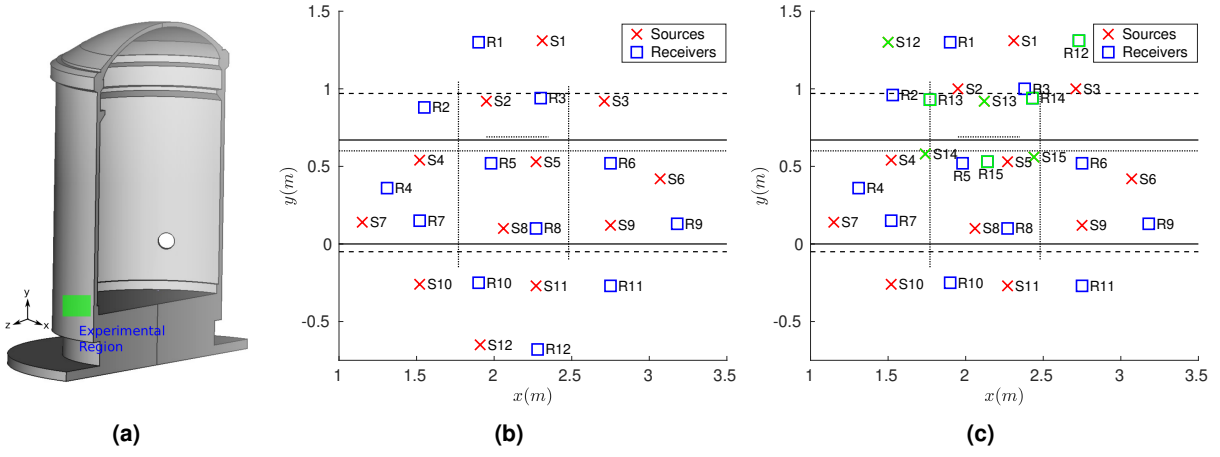


Figure 1. Configuration of the experiment. (a) Sketch of the concrete structure and the experimental region (green square). We focus on the lower corner (the gusset) of the exterior surface of VeRCoRs, a 1/3 replica of a nuclear containment wall. (b) Source and receiver positions in 2017 and 2018. (c) Source and receiver positions in 2019 with new transducer positions in green on the top part of the experimental region (S12 to S15 and R12 to R15). All transducers are glued on the outer surface ($z = 0$) of the structure. The horizontal solid lines represent the change of thickness of the wall. The thickness of the upper part is 40 cm and the middle part (gusset) is 60 cm. The bottom layer is the base slab. The dashed horizontal lines are positions of the construction joint. Dotted lines are positions of cracks on the surface of the wall observed in 2018.

to construct all the source-receiver impulse responses, through deconvolution of recorded waveforms with the chirp source signal. The whole acquisition process takes about 3 minutes, within which the change of concrete can be neglected. The same process is repeated every hour to obtain measurements at different loading states.

The impulse response lasts 4 ms and consists 10000 discrete points. Because of the high diffusion and dissipation of ultrasound in the concrete, we observe that receivers more than one meter away from the source can only record background noise. We check all the signals and choose the interval 1.8 ms – 2.2 ms to estimate the average amplitude of the background noise level.

Apparent velocity change and decorrelation analysis

Let us consider ultrasounds generated and recorded by the same source-receiver pair in two different states: $\phi_1(t)$ and $\phi_2(t)$. The apparent velocity change dV/V_a on the time interval $[t_1, t_2]$ is defined by

$$dV/V_a = \arg \max_{\alpha} \frac{\int_{t_1}^{t_2} \phi_1((1+\alpha)t)\phi_2(t)dt}{\sqrt{\int_{t_1}^{t_2} \phi_1^2((1+\alpha)t)dt \int_{t_1}^{t_2} \phi_2^2(t)dt}},$$

i.e., the amount of stretching that maximizes CC between the signals, and the DC is one minus CC, i.e.,

$$DC = 1 - \max_{\alpha} \frac{\int_{t_1}^{t_2} \phi_1((1+\alpha)t)\phi_2(t)dt}{\sqrt{\int_{t_1}^{t_2} \phi_1^2((1+\alpha)t)dt \int_{t_1}^{t_2} \phi_2^2(t)dt}}.$$

As an example, if the velocity decreases in the second state and if we focus on a peak at t_0 in the wave field ϕ_1 , then the same peak should arrive after t_0 in ϕ_2 . Therefore, to match the peak in these two waveforms, α should be negative. That is to say, a dilation of the time axis (a negative dV/V_a) indicates a decreasing velocity.

To quantitatively study the response of concrete to pressure changes in different regions and to compare the state of the concrete over different years, we compute dV/V_a and DC for three source-receiver pairs between the original state and other states during the inflation-deflation procedure: the top pair (S2-R3 in Fig. 1), the middle pair (S6-R6) and the bottom pair (S10-R10). The time window is chosen to be $[0.16, 0.48]$ ms in this section, which is much larger than those chosen in the following section. We intentionally choose a large interval and the early part of the waveform to stabilize the computation because late-arrival waves vary too much for ultrasound to handle. The apparent velocity change is obtained by interpolating ϕ_1 on a fine mesh of α and finding the one maximizing the inner product of $\phi_1((1+\alpha)t)$ and $\phi_2(t)$.

Fig. 2(c) shows the value of dV/V_a for source-receiver pairs located at the top (in blue), middle (in green) and bottom (in red) zones of the structure, during inflation cycles from 2017 to 2019. When the structure is inflated, stress builds up in concrete, as shown in Fig. B1 and B2 in appendix B, where we plot tangential stress distribution calculated with linear elastic simulations. The stress distribution shows traction in the upper part of the structure. This is consistent with what is observed in Fig. 2(c), which exhibits a decrease of velocity for the source-receiver pair located at the top region. However, the apparent velocity change remains small in the middle and marginal at the bottom, where the simulation shows a constant stress or compression.

We have also checked the uncertainties of the apparent velocity changes. Appendix A describes how the uncertainties are calculated, following the formula introduced by³⁰. These uncertainties are shown as colored areas in Fig. A1, for the source-receiver pair located at the upper region of the structure. One may see that they remain small despite strong apparent velocity changes.

From 2017 to 2019 one notices an increase in the slope of dV/V_a , which suggests that the sensitivity of

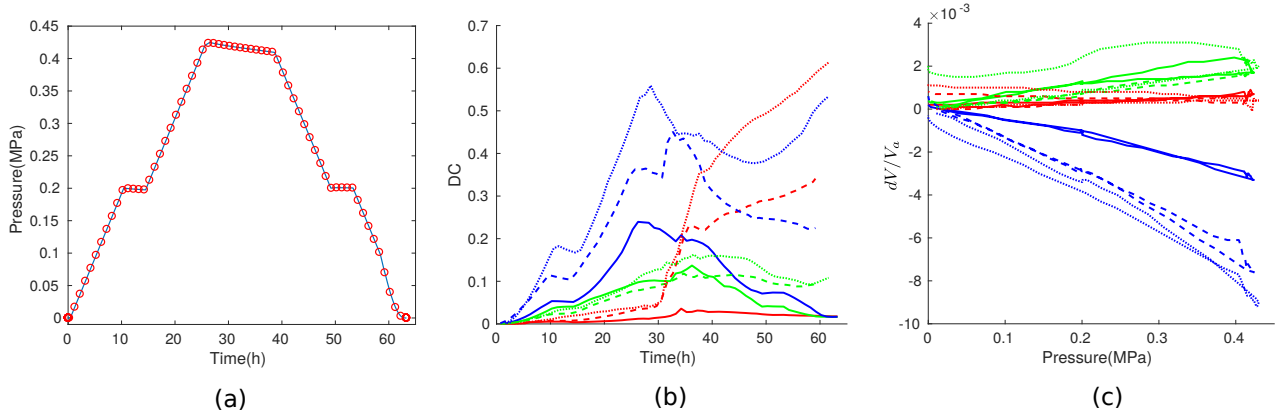


Figure 2. (a) pressure variation during the inflation-deflation procedure. We took the measurement every an hour, during which the pressure has a change of + or - 0.02 MPa except in steady states. (b) DC between the original state and other states; (c) dV/V_a variation with respect to pressure. Blue, green and red lines in (b) and (c) correspond to the top, middle and bottom source-receiver pairs (S2-R3, S6-R6 and S10-R10 in Fig. 1(b)), respectively. Solid, dashed and dotted lines are results from 2017, 2018 and 2019, respectively.

concrete to the same pressure change becomes larger. That is to say, the deterioration of the concrete is more pronounced¹⁹. Another interesting phenomenon is that in 2017 the line during inflation almost overlaps with the line during deflation which means that expansion and contraction of the concrete are fully reversible, because the concrete properties have not evolved significantly between the first ever pressure test in 2017 and the one performed soon after presented here, which is no more the case in 2019. This might be a good criterion to quantify the damaging impact of the pressure tests, and to test the quality of the concrete. Similar conclusions can be drawn for the middle and bottom pairs, though a much lower resolution: the middle region experiences a contraction and the pressure in the bottom region keeps almost unchanged. We leave the precision study of the dV/V_a due to changes in wave speed in the Appendix.

In 2017, the concrete retrieves its initial state after the whole inflation-deflation procedure, as indicated by DC (solid lines) in Fig. 2(b), which is not the case in 2018 and 2019. We conclude from lines with the same color that the change of DC becomes more irreversible as time goes by, which is caused by the cumulative deterioration of the concrete (including micro-cracks and cracks). The large value of DC between the initial and final states implies that the damage induced by pressure changes is permanent: some cracks open and close reversibly while others develop further and the crack surface is altered such that they do not close exactly back to their initial state. What's also interesting is the bottom pair: we do not observe significant pressure changes in the bottom region from dV/V_a , but they do suffer dramatic scattering (or structural) changes (see Fig. 2(b)).

Starting from the 30th hour, there is an increasing of DC for S10-R10, which is due to the following action on the whole structure. In order to estimate the amount of leakage, visually detect the cracks and perform other experiments, during the pressure-steady stage (from around the 30th to 38th hour), soap water is poured from the top of the structure. From our data we conclude that

the impact of the water is more significant for the bottom region of our experimental domain.

3D cartography of velocity and structural changes

The relation between the relative velocity change $\frac{dV}{V}$ and dV/V_a is given by

$$\frac{dV/V_a}{t} = \int \frac{dV}{V}(x) K(s, r, x, t) dx,$$

and the formula connecting the scattering change and DC has a similar form

$$DC = \int \frac{V\sigma(x)}{2} K(s, r, x, t) dx,$$

where V is the average velocity of the ultrasound and σ is the local scattering cross section density. The reader may refer to²² for more details. These two formula share a common sensitivity kernel $K(s, r, x, t)$, which is computed from the diffusive approximation of the coda wave. The sensitivity kernel reflects the probability that a wave emitted at s at time 0 and collected at r at time t has passed through the position x . Here t is in practice the center of the time window where we evaluate dV/V_a and DC experimentally.

In order to solve the integral equations, the medium is divided into equally sized cuboids. The value of the unknown variable inside one cuboid, $\frac{dV}{V}$ or σ , is assumed to be constant and approximated by the value at the center of each cuboid. In our experiment, the size of the cuboids along x , y and z axes is 10 cm, 8 cm and 10 cm, respectively. We choose 13 consecutive time intervals starting from 0.2 ms. Each of them has a length of 0.08 ms. We remove intervals whose average waveform amplitude is no larger than 2.5 times the noise amplitude. The calculating of the sensitivity kernel and integral equation is implemented in 3D. Refer to²³ for a detailed discussion about computing the sensitivity kernel and solving the integral equations.

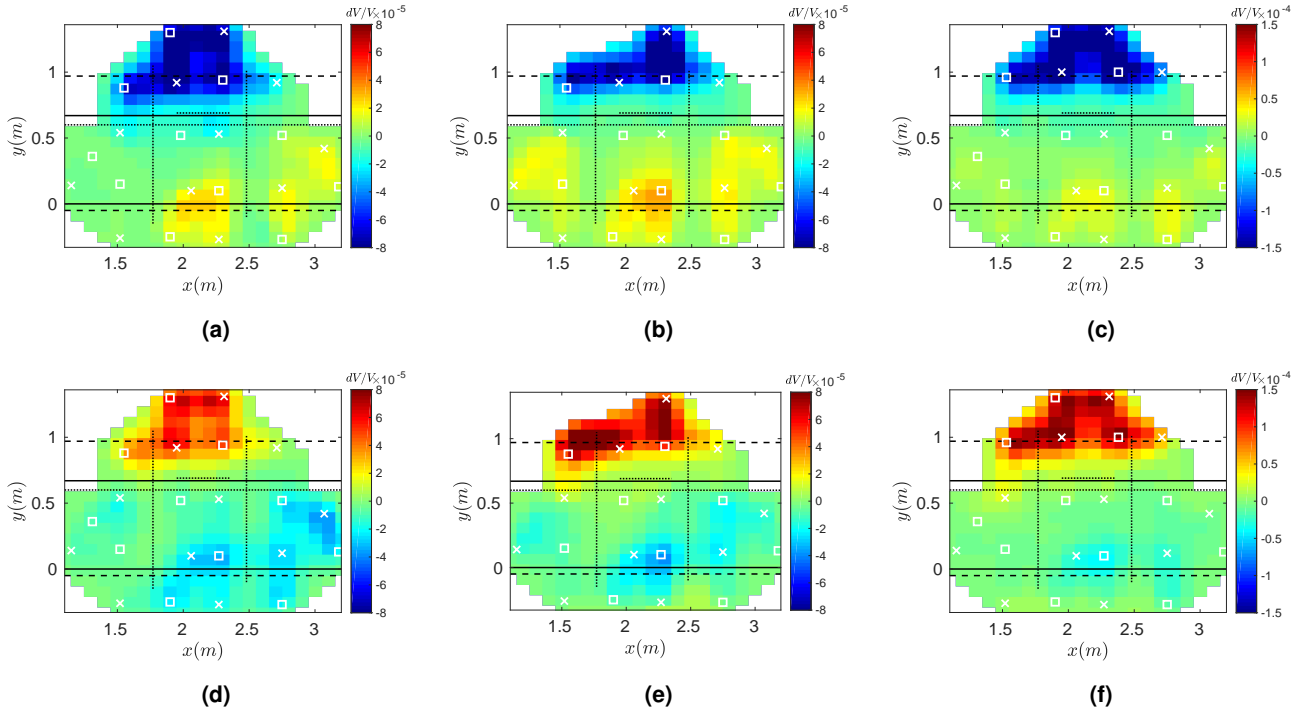


Figure 3. (a)-(c) average relative velocity change between consecutive measurements (one hour apart) at a depth of 5 cm during the second inflation stage in 2017, 2018 and 2019, respectively; (d)-(f) results during the first deflation stage. The white crosses and squares indicate positions of sources and receivers, respectively. Black lines are the same as those in Fig. 1.

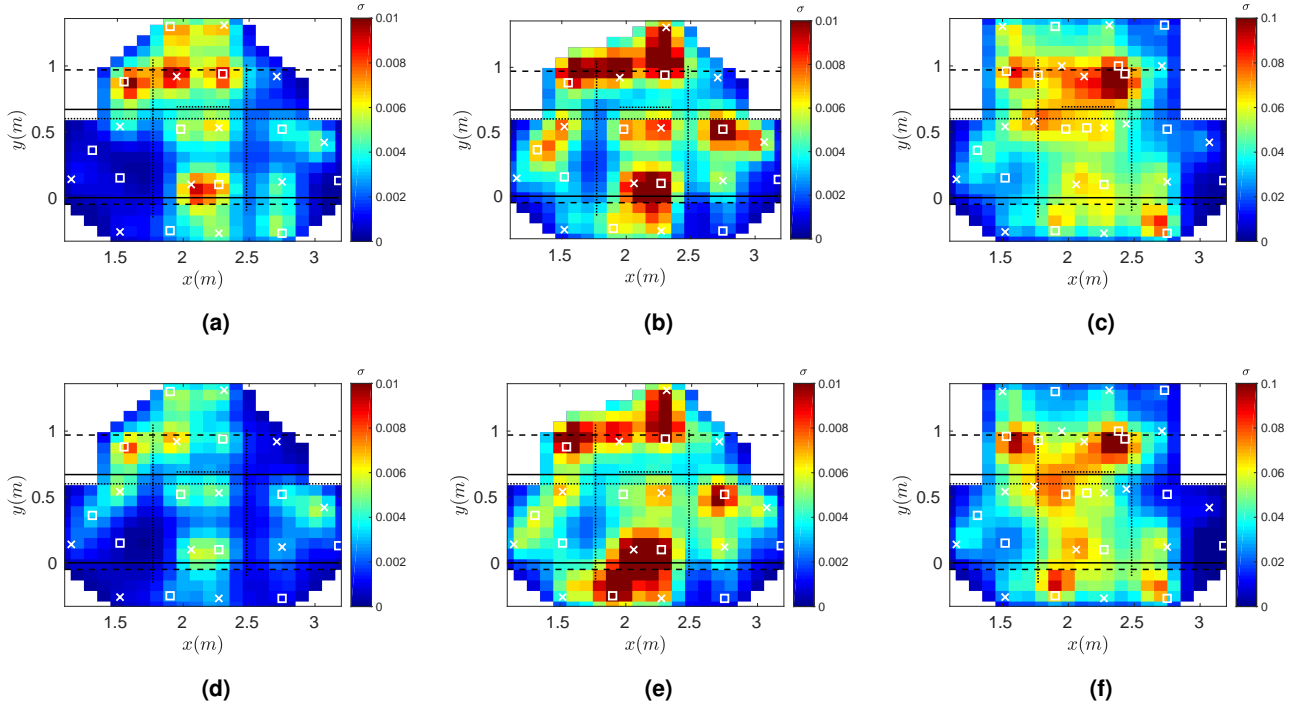


Figure 4. (a)-(c) average structural (scattering) change between two adjacent measurements at the depth of 5 cm during the second inflation stage in 2017, 2018 and 2019, respectively. (d)-(f) results during the first deflation stage. The white crosses and squares indicate positions of sources and receivers, respectively. Black lines are the same as those in Fig. 1.

We compute the velocity change between every two consecutive states and take the average value from all consecutive pairs in the second inflation stage (from 0.21 MPa to 0.41 MPa) and the first deflation stage (from 0.40 MPa to 0.21 MPa) to generate Fig. 3. Each step has, in average, a change of + or - 0.02 MPa. The

decreasing (increasing, respectively) velocity is observed in the inflation stage in the top region (in the lower middle region, respectively), and the opposite phenomenon occurs during the deflation stage. The magnitude in 2019 is much larger than in 2017, which indicates again the cumulative damage of the concrete over years. We only

present velocity changes of the top layer (at a depth of 5 cm from the surface). We obtain similar results for other depth, except a decrease of magnitude and resolution for deeper layers.

Fig. 4 shows the average structural changes, or more precisely the scattering cross section density $\sigma(x, y)$ of the changes, between two consecutive states during the second inflation and first deflation stages. The units (m^2/m^3) can be understood as a density of micro-cracks per volume unit. We observe an increase of scattering change from 2017 to 2019. Our result shows that the most active region is along the top construction joint. We also observe the developing of the crack near dotted lines from 2017 to 2019.

Conclusion and discussion

In this work, we use diffuse ultrasound to study the pressure and structural changes in the gusset area of a 1/3 replica of a nuclear power plant containment wall. Changes are induced by the increase and decrease of the inner pressure. We list the main results below:

1. We are able to image the ultrasonic relative velocity change with a magnitude as small as 10^{-4} thanks to the high sensitivity of diffuse ultrasound.
2. The stretching of diffuse ultrasound and reconstructed velocity change indicate that the concrete near the base is in compression and in traction in the upper region in the inflation process, in agreement with mechanical models.
3. The increase of the slope of dV/V_a versus internal pressure change from 2017 to 2019, in other words the sensitivity of dV/V_a to internal pressure, suggests that the concrete is progressively damaged and weakened. That is to say, the concrete deteriorates over time.
4. Although we do not detect significant pressure change in the base (bottom) region, it could actually also suffer severe cumulative changes. The large DC value between the initial and final states suggests that the concrete does not restore to its initial state during the test, i.e., the damage is permanent and irreversible, at least on the time scale of the test.
5. The reconstructed structural changes (scattering cross section) shows active regions during the inflation-deflation procedure that could correspond to cracking inside the concrete.

Funding

This work was partially funded by the ANR ENDE (PIA 11-RSNR-0009) project, and by the IDEX Université Grenoble Alpes innovation Grant (CND-US).

Appendix A

In³⁰, authors proposed to evaluate the uncertainties of dV/V_a due to the change in wave speed through the

computation of its root mean square

$$\text{rms}(dV/V_a) = \sqrt{\frac{6\sqrt{\frac{\pi}{2}}T}{\omega_c^2(t_2^3 - t_1^3)} \frac{\sqrt{1-CC^2}}{2CC}} \quad (1)$$

For our experiment, the parameters are as follows:

$$\begin{aligned} \omega_c &= 2\pi \times 1.5 \times 10^5 \text{ rad/sec,} \\ T &= \frac{\ln 10}{(2.2 \times 10^5 - 0.8 \times 10^5)\pi}, \\ t_1 &= 1.6 \times 10^{-4} \text{ sec,} \\ t_2 &= 4.8 \times 10^{-4} \text{ sec.} \end{aligned}$$

Application of this formula to data recorded in 2017, 2018 and 2019 at the upper source-receiver pair gives the uncertainty interval $dV/V_a \pm \text{rms}(dV/V_a)$ represented as colored region in Fig. A1.

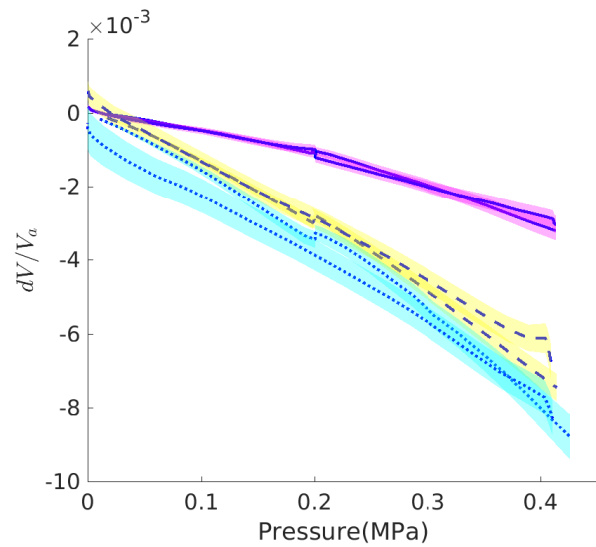


Figure A1. Apparent velocity change calculated in 2017 (solid line), 2018 (dashed line) and 2019 (dotted line) from source-receiver pair at the upper region, and the corresponding uncertainties evaluated from Eq. (1) (colored region).

Appendix B

Here we evaluate numerically the state of stress inside the concrete around the gusset. We perform elastic linear numerical simulations using the ASTER code³¹, without taking into account the possible role of cracks. For clarity, we only represent the difference of stress between the initial state (additional internal pressure 0 MPa) and the final state (internal pressure 0.43 MPa). Fig. B1 and B2 represent a 2D vertical cut and a vertical profile of this tangential stress change. Positive values correspond to traction, where cracks are expected to develop and open, and where dV/V_a is expected to be negative. Negative values of stress correspond to compression areas, where dV/V_a are expected to be positive. Experimental results of dV/V_a are perfectly in agreement with this mechanical simulations, demonstrating the ability of dV/V_a obtained from ultrasonic coda waves to cartography the state of stress inside the structure.

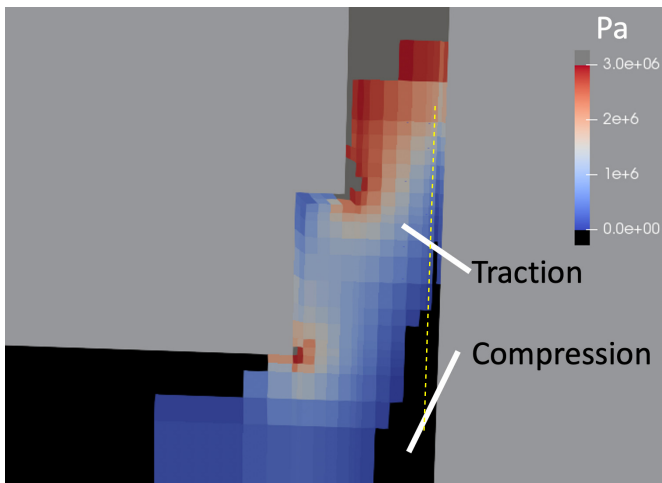


Figure B1. Numerical simulation of stress around the gusset (vertical cut). We represent here the difference in tangential stress from the initial state (no internal pressure) to the plateau at 0.4 MPa. The colored areas indicate traction (from 0 to 0.3 MPa approximately). Black color indicates compression or neutral areas. The yellow vertical dashed line is the position where we plot Fig. B2.

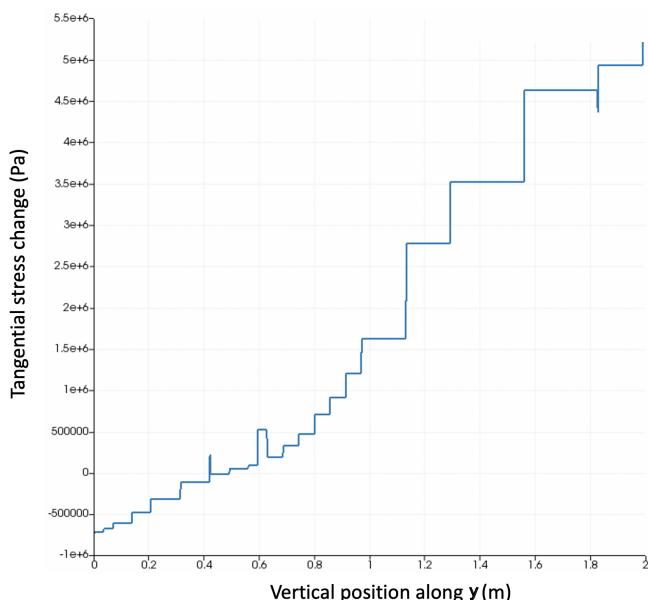


Figure B2. Tangential stress difference between the initial (0 MPa) and final (0.43 MPa) state along a vertical line (y-axis) at a 5 cm depth inside the concrete (from the outside surface). Negative values hold for compression, positive values for traction.

References

- République Française. Décret No. 2007-1557 du 2 November 2007. <https://www.legifrance.gouv.fr/jorf/id/JORFTEXT000000469544>.
- Masson B and Alliard PM. Objectives and design of the new experimental program vercors based on a 1/3 scaled PWR containment building. *TINCE 2013* 2013; .
- Mathieu J, Charpin L, Sémété P et al. Temperature and humidity-driven ageing of the vercors mock-up. In *Computational Modelling of Concrete Structures: Proceedings of the Conference on Computational Modelling of Concrete and Concrete Structures (EURO-C 2018)*, volume 215.
- Henault JM, Laviron P, Desforges S et al. How to characterize the airtightness of containment structure; overview of monitoring techniques tested on VerCoRs mock up. In *Congres on Technological Innovations in Nuclear Civil Engineering (TINCE), France, Paris-Saclay*.
- Wegler U and Sens-Schönfelder C. Fault zone monitoring with passive image interferometry. *Geophysical Journal International* 2007; 168(3): 1029–1033.
- Brenguier F, Campillo M, Hadziioannou C et al. Postseismic relaxation along the san andreas fault at parkfield from continuous seismological observations. *science* 2008; 321(5895): 1478–1481.
- Grêt A, Snieder R, Aster RC et al. Monitoring rapid temporal change in a volcano with coda wave interferometry. *Geophysical Research Letters* 2005; 32(6).
- Sens-Schönfelder C and Wegler U. Passive image interferometry and seasonal variations of seismic velocities at merapi volcano, indonesia. *Geophysical research letters* 2006; 33(21).
- Brenguier F, Shapiro NM, Campillo M et al. Towards forecasting volcanic eruptions using seismic noise. *Nature Geoscience* 2008; 1(2): 126–130.
- Poupinet G, Ellsworth W and Frechet J. Monitoring velocity variations in the crust using earthquake doublets: An application to the calaveras fault, california. *Journal of Geophysical Research: Solid Earth* 1984; 89(B7): 5719–5731.
- Snieder R, Grêt A, Douma H et al. Coda wave interferometry for estimating nonlinear behavior in seismic velocity. *Science* 2002; 295(5563): 2253–2255.
- Snieder R. The theory of coda wave interferometry. *Pure and Applied geophysics* 2006; 163(2-3): 455–473.
- Lobkis OI and Weaver RL. Coda-wave interferometry in finite solids: Recovery of P-to-S conversion rates in an elastodynamic billiard. *Physical review letters* 2003; 90(25): 254302.
- Planès T, Larose E, Rossetto V et al. Imaging multiple local changes in heterogeneous media with diffuse waves. *The Journal of the Acoustical Society of America* 2015; 137(2): 660–667.
- Larose E, de Rosny J, Margerin L et al. Observation of multiple scattering of khz vibrations in a concrete structure and application to monitoring weak changes. *Physical Review E* 2006; 73(1): 016609.
- Larose E and Hall S. Monitoring stress related velocity variation in concrete with a 2×10^{-5} relative resolution using diffuse ultrasound. *The Journal of the Acoustical Society of America* 2009; 125(4): 1853–1856.
- Schurr DP, Kim JY, Sabra KG et al. Damage detection in concrete using coda wave interferometry. *NDT & E International* 2011; 44(8): 728–735.
- Hilloulin B, Zhang Y, Abraham O et al. Small crack detection in cementitious materials using nonlinear coda wave modulation. *NDT & E International* 2014; 68: 98–104.
- Planès T and Larose E. A review of ultrasonic coda wave interferometry in concrete. *Cement and Concrete Research* 2013; 53: 248–255.
- Pacheco C and Snieder R. Time-lapse travel time change of multiply scattered acoustic waves. *The Journal of the Acoustical Society of America* 2005; 118(3): 1300–1310.
- Larose E, Planes T, Rossetto V et al. Locating a small change in a multiple scattering environment. *Applied Physics Letters*

- 2010; 96(20): 204101.
22. Planès T, Larose E, Margerin L et al. Decorrelation and phase-shift of coda waves induced by local changes: multiple scattering approach and numerical validation. *Waves in Random and Complex Media* 2014; 24(2): 99–125.
 23. Xue Q, Larose E and Moreau L. Locating structural changes in a multiple scattering domain with an irregular shape. *The Journal of the Acoustical Society of America* 2019; 146(1): 595–602.
 24. Kanu C and Snieder R. Numerical computation of the sensitivity kernel for monitoring weak changes with multiply scattered acoustic waves. *Geophysical Supplements to the Monthly Notices of the Royal Astronomical Society* 2015; 203(3): 1923–1936.
 25. Zhang Y, Planes T, Larose E et al. Diffuse ultrasound monitoring of stress and damage development on a 15-ton concrete beam. *The Journal of the Acoustical Society of America* 2016; 139(4): 1691–1701.
 26. Zhan H, Jiang H and Jiang R. Three-dimensional images generated from diffuse ultrasound wave: detections of multiple cracks in concrete structures. *Structural Health Monitoring* 2020; 19(1): 12–25.
 27. Zhang Y, Larose E, Moreau L et al. Three-dimensional in-situ imaging of cracks in concrete using diffuse ultrasound. *Structural Health Monitoring* 2018; 17(2): 279–284.
 28. Charpin L, Niepceron J, Corbin M et al. Ageing and air leakage assessment of a nuclear reactor containment mock-up: VERCORS 2nd benchmark. *Nuclear Engineering and Design* 2021; 377: 111136.
 29. Zhang Y, Abraham O, Grondin F et al. Study of stress-induced velocity variation in concrete under direct tensile force and monitoring of the damage level by using thermally-compensated coda wave interferometry. *Ultrasonics* 2012; 52(8): 1038–1045.
 30. Weaver RL, Hadziioannou C, Larose E et al. On the precision of noise correlation interferometry. *Geophysical Journal International* 2011; 185(3): 1384–1392.
 31. Electricité de France. Finite element *code_aster*, structures and thermomechanics analysis for studies and research. Open source on www.code-aster.org, 1989–2021.